AGU ADVANCING EARTH AND SPACE SCIENCE

Geophysical Research Letters

RESEARCH LETTER
10.1029/2020GL090299

Kauri Tree-Ring Stable Isotopes Reveal a Centennial Climate Downturn Following the Antarctic Cold Reversal in New Zealand

M. Pauly[1,2,3], C. S. M. Turney[4], J. G. Palmer[4], U. Büntgen[5,6], A. Brauer[1], and G. Helle[1,2]

[1]Section "Climate Dynamics and Landscape Evolution", GFZ German Research Centre for Geosciences, Potsdam, Germany, [2]Department of Earth Sciences, Section of Palaeontology, Free University of Berlin, Berlin, Germany, [3]School of Science, Bath Spa University, Bath, UK, [4]School of Biological, Earth and Environmental Sciences, Palaeontology, Geobiology and Earth Archives Research Centre (PANGEA), University of New South Wales, Sydney, Australia, [5]Department of Geography, University of Cambridge, Cambridge, UK, [6]Global Change Research Centre and Masaryk University, Brno, Czech Republic

Key Points:

- Dual isotope ($\delta^{18}O_{cel}$, $\delta^{13}C_{cel}$) tree-ring stable isotope chronologies (KAU-ISO) were developed from New Zealand kauri trees, covering 13,020–11,850 cal BP
- A simultaneous downturn in all tree-ring proxies was established covering 250 years (Kauri Downturn = KD)
- The records presented provide new high-resolution evidence of hydroclimate conditions in NZ at the end of the Late Glacial

Supporting Information:

- Supporting Information S1

Correspondence to:
M. Pauly,
m.pauly@bathspa.ac.uk

Citation:
Pauly, M., Turney, C. S. M., Palmer, J. G., Büntgen, U., Brauer, A., & Helle, G. (2021). Kauri tree-ring stable isotopes reveal a centennial climate downturn following the Antarctic Cold Reversal in New Zealand. *Geophysical Research Letters*, *48*, e2020GL090299. https://doi.org/10.1029/2020GL090299

Received 12 AUG 2020
Accepted 16 DEC 2020

Abstract The dynamics of the Late Glacial have been demonstrated by numerous records from the Northern Hemisphere and far fewer from the Southern Hemisphere (SH). SH paleoclimate records reveal a general warming trend, interrupted by a deglaciation pause Antarctic Cold Reversal (ACR; ~14,700–13,000 cal BP). Here, we present decadal tree-ring stable isotope chronologies ($\delta^{18}O$, $\delta^{13}C$) from New Zealand (NZ) subfossil kauri trees ($n = 6$) covering the post-ACR millennium from 13,020 to 11,850 cal BP. We find a distinct, simultaneous downturn (~12,625–12,375 cal BP) in all tree-ring proxies paralleling regional tree growth declines, suggesting a widespread climate deterioration. This downturn was characterized by sustained high precipitation, low temperatures, and high relative humidity in NZ with incoming weather fronts from the South Ocean. Despite these promising results, questions remain about what drove the Kauri Downturn and how the hydroclimatic conditions were altered during this time period.

1. Introduction

1.1. The Late Glacial

Significant attention in paleoclimate research has focused on the transitional period between the last glaciation and the current Holocene interglacial, known at the Late Glacial (~14,700–11,600 cal BP). In the Northern Hemisphere (NH), the gradual warming was interrupted by numerous fast transitions to cold episodes of various lengths. The most prominent millennium-long cold reversal to near glacial conditions is evidenced in Greenland ice core $\delta^{18}O$ and deuterium excess (GS-1; Figure 1h). This led to significant palynological changes in continental Europe characterizing the so-called Younger Dryas (YD) period (Brauer et al., 2000; Rach et al., 2014; Steffensen et al., 2008). The Southern Hemisphere (SH), however, tells a very different story, with the gradual warming continuing until the warm Holocene, with the exception of a brief warming pause during the Antarctic Cold Reversal (ACR, ~14,700–13,000 cal BP; Blunier et al., 1997; Pedro et al., 2011; WAIS 2015; Figure 1g) and various decadal oscillations demonstrated in New Zealand (NZ) records (Barrell et al., 2013). Similar hemispheric divergences have been discovered over long-term Glacial-Interglacial cycles across the Quaternary period (Crowley, 1992), evidenced as SH warming leading the NH during glacial terminations; due in part to slower melting of NH ice sheets, greatly impacting hemispheric temperatures (Kawamura et al., 2007).

The abrupt NH cold reversal (Younger Dryas onset/beginning of GS-1) at the end of the Late Glacial has been hypothesized to be a result of weakening of the Atlantic meridional overturning circulation (AMOC) (Carlson & Clark, 2012; Renssen et al., 2015); an Atlantic ocean current system characterized by a northward flow of tropical surface warm waters, which cool and sink in the North Atlantic and eventually reroute back south along the coast of North America. AMOC weakening can occur as a result of freshening of the North Atlantic (due to ice melt), decelerating the thermosaline-modulated oceanic circulation system. Such weakening would theoretically block warm tropical waters from entering the North Atlantic allowing for reestablishment of sea ice (and GS-1/YD glacial conditions), while concurrently impeding cool deep-water

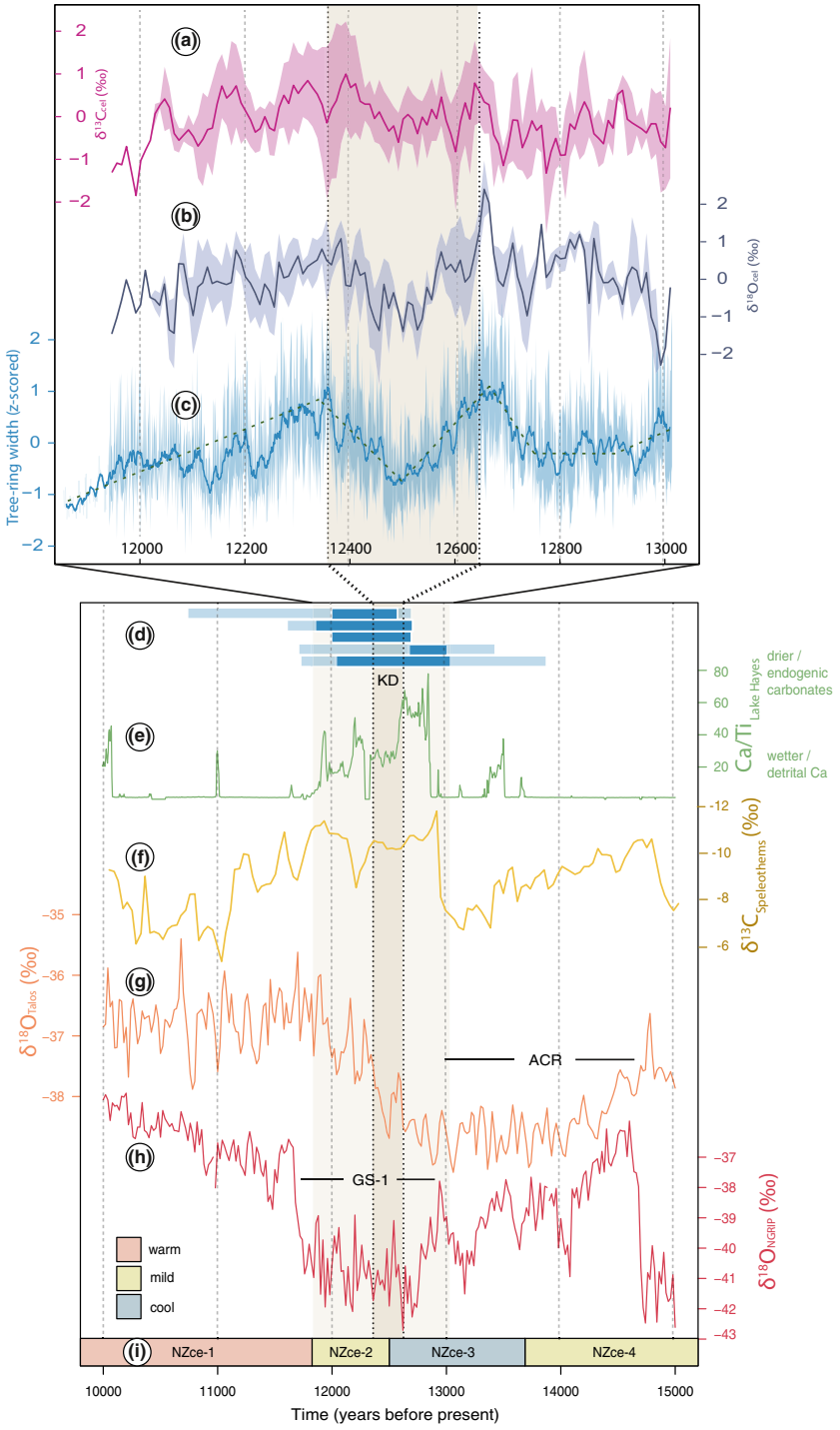

Figure 1. A high-resolution view of the Late Glacial in the Southern Hemisphere. Decadal *z*-scored chronology (KAU-ISO) of (a) $\delta^{13}C_{cel}$ and (b) $\delta^{18}O_{cel}$ and with standard deviation shaded ($n_{trees} = 6$); (c) tree-ring width of full Towai chronology (Palmer et al., 2017) subsetted to length of KAU-ISO (13,020–11,850 cal BP). Kauri Downturn (KD) shaded. (d) Bars represent individual kauri trees used in this study, with the full length of individual trees in light blue and decadal stable isotope (KAU-ISO) subset in dark blue. (e) Lake Hayes sediment record of Ca/Ti (Hinojosa et al., 2019); (f) speleothem $\delta^{13}C$ from New Zealand (Whittaker et al., 2008); (g) Antarctic (Talos Dome; Pedro et al., 2011); and (h) Greenland (NGRIP, Rasmussen et al., 2014) ice core $\delta^{18}O$ during the Late Glacial with the Antarctic Cold Reversal (ACR) and Greenland Stadial 1 (GS-1; equivalent to the pollen defined Younger Dryas) indicated. Climate stages according to (i) Kaigo Bog stratigraphy (Hajdas, 2006; Newnham & Lowe, 2000), including the Late-Glacial mild episode (NZce-4), the Late-Glacial cool episode (NZce-3), the pre-Holocene amelioration (NZce-2), and the Holocene interglacial (NZce-1); time according to GICC05 (years before 1950).

upwelling in the south Atlantic causing SH warming and thus a bipolar divergence in climate. Changes in AMOC activity are hypothesized to be further compounded in the SH by shifts in the southern westerly wind belt and associated ocean currents as the Intertropical Convergence Zone (ITCZ) oscillated across latitudes (Denton et al., 2010). Thus, climate change induced by variations in AMOC and related ocean circulation can lead to a complex and divergent set of conditions between regions and hemispheres (Figure 1), also demonstrated in the coupled atmosphere-ocean general circulation model, TraCE-21ka (Figure S1); referred to as the "bipolar seesaw" (Stocker et al., 1998)

1.2. LG Climate Downturns. Southern Versus Northern Hemisphere

While the triggers of LG cold episodes are still under debate, numerous climate records in the NH have been established to understand the impact and regionality of cold episodes across the Late Glacial. These records (Brauer et al., 2000; Lauterbach et al., 2011; Merkt & Müller, 1999; von Grafenstein et al., 1999) demonstrate long-term and low-frequency temperature variability similar to Greenland ice cores (Rasmussen et al., 2014; Steffensen et al., 2008), with some regional differences in the rate, magnitude, and timing of climate events (e.g., Pauly et al., 2018; Rach et al., 2014). Conversely, the southern hemisphere has far fewer paleoclimate records available covering this interesting climate period, with only a handful of relevantly high (decadal) temporal resolution (e.g., De Deckker et al., 2012, Hajdas et al., 2006; Figure 1).

During the YD phase, when the NH plunged into cold conditions, Antarctica experienced a warming trend. Antarctic ice core $\delta^{18}O$ (e.g., Pedro et al., 2011), reconstructed Southern Ocean sea surface temperature (Correge et al., 2004) and New Zealand glacier retreat (Kaplan et al., 2010) argue for steadily increasing temperatures between ~12,900 and 11,800 cal BP in the SH. Southern Australia ocean core data suggest this warm phase was regionally modulated by an oscillating Subtropical Front (STF), permitting a millennial flickering of the Leeuwin Current (LC) strength across southern Australia past Tasmania (De Deckker et al., 2012). This STF activity ultimately impacted regional temperature and precipitation patterns during distinct phases. During one such interval (~12,500–12,380 cal BP), Tasmanian huon pine (*Lagarostrobus franklinii*) and New Zealand kauri (*Agathis australis*) trees show significant centennial-long growth depressions (Hua et al., 2009; Palmer et al., 2016; Figure 1c) which may be related to a changed state of the midlatitude Southern Ocean and related El Niño-Southern Oscillation (ENSO) activity (Palmer et al., 2016). Locally, this interval parallels a conversion from a dry ACR to relatively wet conditions at Lake Hayes in South Island NZ (Hinojosa et al., 2019; Figure 1e). In North Island, this short period represents a transition from the Late-Glacial cool episode (NZce-3) to the pre-Holocene amelioration (NZce-2) according to Kaipo bog stratigraphy (Figure 1i; Barrell et al., 2013; Hajdas, 2006; Newnham & Lowe, 2000) as well as wet, cool conditions recorded in Ruakuri Cave speleothems during Heinrich Event 0 (Whittaker et al., 2008; Figure 1f). Regionally, a short-term depletion in Talos ice core $\delta^{18}O$ (Figure 1g; ~12,580–12,380 cal BP), and Law ice core $\delta^{18}O$ (Pedro et al., 2011; ~12,540–12,320 cal BP) may provide hints of the climate deterioration in Eastern Antarctica; although it generally appears to be independent of the Atlantic and West Antarctic regions, with no significant signal visible in Western Antarctica (EDML, Siple and Bryd ice cores; Pedro et al., 2011). Palmer et al. (2016) hypothesized this tree growth downturn was followed by a strengthening of ENSO expression in the region and/or solar variability. However, due to the limited climate records existing over this period and the limited age control of New Zealand records, the climatological characteristics of this centennial-duration event remain under debate.

1.3. Kauri Trees as a Climate Archive

New Zealand kauri (Figures 2a and 2b) trees are southern hemisphere conifers which can grow for multiple millennia (Palmer et al., 2016) and thrive in warm-temperate lowlands regions. Due to their long lifespan, annual rings and sensitivity to summer climate indices, Kauri trees are an important bioarchive. Studies include living kauri trees (Fowler et al., 2004; Ogden & Ahmed, 1989), archeological timber (Boswijk et al., 2006), as well as ancient material (e.g., Lorrey & Ogden, 2005; Palmer et al., 2016; Turney et al., 2010) dating as far as 60,000 years before present. Tree-ring width chronologies of kauri have demonstrated a connection with ENSO activity in modern times (Fowler et al., 2007, 2000) as well as during the Holocene (Fowler et al., 2012) and the Late Glacial (Palmer et al., 2016).

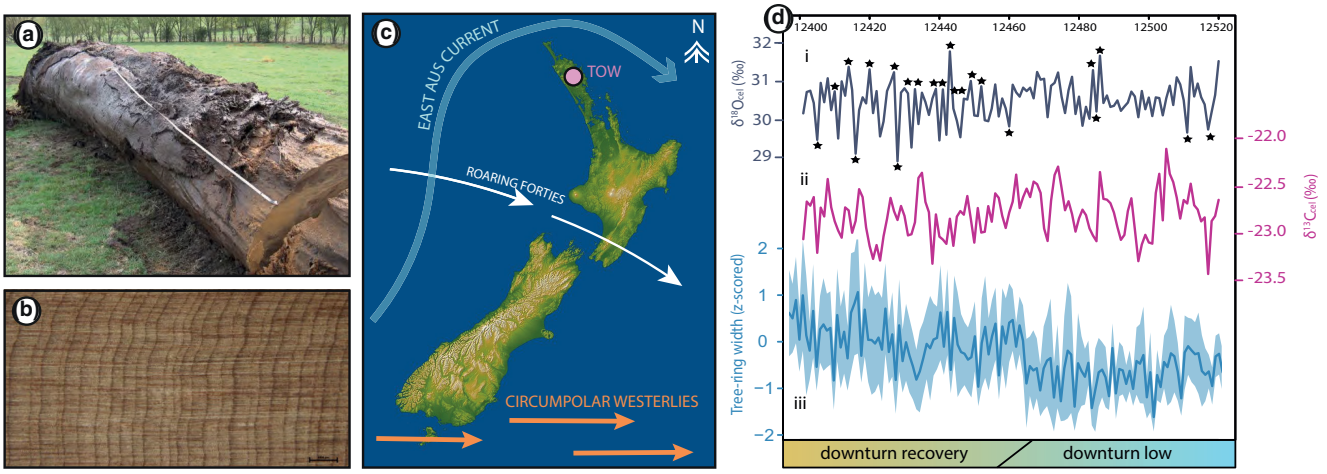

Figure 2. Kauri tree characteristics, site, and annual variability. (a) Stump of kauri tree found on Towai farm; (b) close-up of individual tree rings; (c) climate situation in New Zealand with site location (TOW) indicated; (d) annual (i), $\delta^{18}O_{cel}$ (ii), $\delta^{13}C_{cel}$ (iii), and tree-ring width (*z*-scored) of a single tree during the latter half of the Kauri Downturn; stars represent annual variability >1‰.

The sensitivity of kauri to summer season (November-February; NDJF) hydroclimate indices have been further explored through stable isotope analysis of modern kauri cellulose (e.g., Brookman, 2014; Lorrey et al., 2016; supporting information S1). Brookman (2014) demonstrated the concurrent sensitivity of $\delta^{18}O$ and $\delta^{13}C$ from kauri tree-ring cellulose ($\delta^{13}C_{cel}$, $\delta^{18}O_{cel}$) to various climate parameters in the summer, including positive correlations to mean temperature ($r_o = 0.70$, $r_c = 0.89$), solar radiation ($r_o = 0.64$, $r_c = 0.89$) and soil moisture ($r_o = 0.71$, $r_c = 0.84$), as well as negative correlations to rainfall ($r_o = -0.33$, $r_c = -0.22$) and relative humidity ($r_o = -0.41$, $r_c = -0.65$). Lorrey et al. (2016, 2018) also found a correlation between $\delta^{18}O_{cel}$ and the SOI indicating that kauri $\delta^{18}O_{cel}$ may be a useful proxy of past ENSO conditions. While both $\delta^{18}O_{cel}$ and $\delta^{13}C_{cel}$ in kauri tend to be similarly sensitive to the above-mentioned climate variables, age-related offsets as well as divergences in microclimate conditions can introduce complexities into the $\delta^{13}C_{cel}$ record (Brookman, 2014) as described in other Late Glacial records (Pauly et al., 2020).

By using kauri tree-ring stable isotopes, we aim to investigate the hydroclimate state of North Island during the post-ACR millennium (13,020–11,850 cal BP) and identify the radiation of ocean-atmospheric dynamics and expression of ENSO in the SH by exploring connections amidst other regional records. Using a dual stable isotope modeling approach, we analyze $\delta^{18}O$ and $\delta^{13}C$ to interpret the growing season climate conditions present before, during and after a distinct growth depression (~12,625–12,375 cal BP, Figure 1c).

2. Materials and Methods

2.1. Subfossil Kauri Chronology

Here, we present a dual stable isotope chronology (carbon and oxygen) developed from tree-ring cellulose extracted from subfossil trees discovered near Towai in Northland, New Zealand (35°30.3930°S, 174°10.3760 E; Figure 2c; supporting information S2). A subset of trees ($n_{trees} = 6$) has been chosen (based on a minimum required to develop a strong climate signal from $\delta^{18}O_{cel}$; Lorrey et al., 2016) from a floating tree-ring chronology (Towai), which covers 13,134–11,694 cal BP ($n_{trees} = 37$, 1σ error of ±7 years; Hogg et al., 2016).

This period spans the Greenland Isotope defined GS-1 (Rasmussen et al., 2014) and pollen defined NH Younger Dryas (e.g., Björck et al., 1998), immediately following the SH Antarctic Cold Reversal (ACR) (Figure 1) and spanning the SH "Late-Glacial cool episode" into the "pre-Holocene amelioration" (Barrell et al., 2013) defined by NZ bog pollen (Hajdas et al., 2006; Lowe et al., 2008, 2013; Newnham & Lowe, 2000).

The stable isotope chronology (KAU-ISO) is of decadal resolution with a sample replication of 4–6 trees for the majority of the chronology (56%; 670 years), with some periods having a replication of 3 trees (28%; 280 years) and even less with a replication of 1–2 (15%; 160 years) (Figure 1d). The subset of trees was

chosen for this work as an initial investigation into the potential to reconstruct climate during the Late Glacial with kauri trees.

The tree-ring width chronology (Palmer et al., 2016) with which this dendroisotope data was developed, hypothesized a connection between a distinct growth depression (~12,625–12,375 cal BP) and subsequent increased intensity in ENSO activity. Trees used here were growing before, during and after this peculiar 250-years long growth depression (Palmer et al., 2016), which we aim to further explore in this study.

2.2. Cellulose Extraction and Stable Isotope Analysis

Cellulose was extracted from wholewood material of 10-years blocks of tree rings (Schollaen et al., 2017; Wieloch et al., 2011) from individual trees covering 13,020 to 11,850 cal BP, which is a subset of the Towai tree-ring chronology. Annual stable isotopes were also measured from an individual tree, covering mid-point of the growth depression, between 12,520 and 12,400 cal BP (Figure 2d). The samples were homogenized and freeze-dried prior to being weighed and packed (silver capsules (ø3.3 × 4 mm) for stable isotope measurement (Delta V, Thermofisher Scientific Bremen; coupled with TC/EA HT at 1,400°C). The measurements were not pooled between trees, only within the 10-years blocks. Results were compared against international and lab-internal reference material (IAEA-CH3, IAEA-CH6 and Sigma-Aldrich Alpha-Cellulose) using two reference standards with widespread isotopic compositions for a single-point normalization (Paul e al., 2007). Final isotope ratios are given in δ value, relative to VSMOW ($\delta^{18}O$) and VPDB ($\delta^{13}C$), with replication reproducibility of ±0.3‰ ($\delta^{18}O$) and ±0.15‰ ($\delta^{13}C$).

2.3. TraCE-21ka Climate Model Outputs

The time interval covered by KAU-ISO was investigated using TraCE-21ka, a coupled atmosphere-ocean general circulation model—which simulates global climate evolution between the Late Glacial Maximum (LGM: 21,000 years before present) to modern times—using the Community Climate System Model version 3 (CCSM3). Three periods of time were examined: (1) predownturn (12,800 cal BP), (2) Kauri Downturn (12,500 cal BP), and (3) postdownturn (12,200 cal BP), and four climate variables: annual (1) relative humidity, (2) precipitation, (3) temperature, and (4) sea level pressure. The modeling was completed over the SH summer season (November-February), when kauri trees exhibit growth (Ecroyd, 1982). Climate model outputs were visualized using PaleoView v1.5.1 with a user defined geographic region (covering Australia, New Zealand and a portion of the Southern Ocean) and changes relative to 10,000 cal BP.

3. Results

3.1. Stable Isotope and Tree-Ring Chronologies

3.1.1. Decadal Stable Isotope Record (KAU-ISO)

Stable oxygen ($\delta^{18}O_{cel}$) and carbon ($\delta^{13}C_{cel}$) records of tree-ring cellulose average ~30.6‰ and ~−22.0‰ with ranges of 4.3‰ (28.3–32.6‰) and 3.8‰ (−20.3−24.1‰) and interdecadal variability of 0.66‰ and 0.37‰, respectively. Inter-tree correlation for $\delta^{18}O_{cel}$ and $\delta^{13}C_{cel}$ is not consistent; ranging between −0.76 and +0.88 for $\delta^{18}O_{cel}$ and −0.44 to +0.80 for $\delta^{13}C_{cel}$ (Table S1 and Figure S2).

Decadal mean $\delta^{18}O_{cel}$ and $\delta^{13}C_{cel}$ records were developed from the individual tree-ring records with an average standard deviation of 0.89 for $\delta^{18}O_{cel}$ and 0.70 for $\delta^{13}C_{cel}$. Correlations between mean $\delta^{18}O_{cel}$ and $\delta^{13}C_{cel}$ are strongly positive during much of the data set, with 38% of the data set demonstrating correlation coefficients above +0.4, a high of +0.82 and absolute average of 0.36 (Figure S2).

During the first 350 years of the chronology (~13,000–12,650 cal BP), mean $\delta^{18}O_{cel}$ exhibits an increasing trend with a peak at ~12,650–12,640 cal BP (Figure 1b), while mean $\delta^{13}C_{cel}$ demonstrates a plateau within a relatively negative anomaly with a similar (albeit less extreme) peak at 12,640 cal BP (Figure 1a). Similar to the previously reported tree-ring width downturn (Palmer et al., 2016; Figure 1c), $\delta^{18}O_{cel}$ and $\delta^{13}C_{cel}$ from KAU-ISO show concurrent and significant depletions between ~12,630 and 12,380 cal BP. This set of depletions begin with a peak (maximum of the entire sequence for $\delta^{18}O_{cel}$) around 12,630 cal BP, followed by a steady decline, with deepest point centred ~12,450 cal BP. This event sequence will hereafter be

referred to as the "Kauri Depression" (KD). All tree-ring parameters (width, $\delta^{18}O_{cel}$, $\delta^{13}C_{cel}$) recover, peaking at ~12,380 cal BP and then continue slow decline until the end of the chronology at 11,850 cal BP.

Mean inter-tree correlations for $\delta^{18}O_{cel}$ are higher during the downturn (average = 0.22, range = −0.07 to +0.55), compared with predownturn and postdownturn; $average_{pre}$ = −0.23, $range_{pre}$ = −0.76 to +0.07, $average_{post}$ = +0.07, $range_{post}$ = −0.22 to +0.28. Conversely, inter-tree correlations for $\delta^{13}C_{cel}$ are equivalent predownturn and during downturn ($average_{pre}$ = 0.13, $range_{pre}$ = −0.44 to +0.80, $average_{downturn}$ = 0.13, $range_{downturn}$ = −0.26 to +0.48, respectively) and relatively higher postdownturn (average = +0.28, $range_{post}$ = −0.27 to +0.64). Slightly higher inter-tree correlations have been found modern kauri stable isotope chronologies of $\delta^{18}O_{cel}$ and $\delta^{13}C_{cel}$, with a correlation of 0.21–0.64 for $\delta^{18}O_{cel}$ (Brookman, 2014; Lorrey et al., 2016) and 0.35 for $\delta^{13}C_{cel}$ (Brookman, 2014).

3.1.2. Annual Stable Isotope Record (KAU-ISO)

Dual isotopes of a single tree were analyzed covering the latter half of the KD (12,520–12,400 cal BP) to provide information on the interannual variability of $\delta^{18}O_{cel}$ and $\delta^{13}C_{cel}$ during this climate "event" (Table S2). This tree displayed a range of $\delta^{18}O_{cel}$ values of only 2.9‰ (28.9‰–31.8‰), which is much more limited than modern kauri $\delta^{18}O_{cel}$ values which demonstrate an 8‰ range (28.‰8–36.8‰) according to Brookman (2014). Based on similarities between the absolute values of the isotopic records, tree species, and location, we assume similar seasonal trends identified in Brookman (2014) would also impact the annual data set presented in this study.

3.2. Climate Model

While precipitation and relative humidity can be estimated from the kauri records in this study, information on temperature and sea level pressure, as well as spatial trends of all parameters, were further investigated using Paleoview software to visualize TRaCE21ka data. The TRaCE21ka model outputs confirm that a phase of high relative humidity and high precipitation in SH summer (NDJF) occurred in NZ during the downturn (~12,500 cal BP) compared to predownturn and postdownturn (12,800 cal BP and 12,200 cal BP, respectively), matching the results of KAU-ISO.

4. Discussion

4.1. Stable Isotope Chronologies

The decadal stable isotope chronologies (KAU-ISO, 13,020–11,850 cal BP) from kauri tree rings reflected similar means and ranges compared to modern studies (Brookman, 2014). Inter-tree correlations varied throughout the record (Figure S1), potentially due to the pooling of decadal tree rings within individual trees; pooling has been shown to hide bias of individual trees which deviate from the population signal (Liñán et al., 2011). Trees showed more significant correlations between individual trees for $\delta^{13}C_{cel}$ measurements over $\delta^{18}O_{cel,}$ in contrast to other subfossil (Pauly et al., 2018, 2020) stable isotope studies, which generally show stronger population signals in $\delta^{18}O_{cel}$ data. Despite individual tree differences, mean $\delta^{18}O_{cel}$ and $\delta^{13}C_{cel}$ demonstrate strong correlations (38% of chronology >0.4; Figure S2), reflecting a set of interdependent variables within the climate system and similar long-term trends.

Annual values of $\delta^{18}O_{cel}$ tend to be more enriched (mean = 30.5‰) than concurrent decadal $\delta^{18}O_{cel}$ values (mean = 29.7‰). This is likely due to the temporal bundling of depleted rainfall (low $\delta^{18}O$) conditions as a result of persistent, widespread, and low-frequency (decadal) atmospheric oscillations occurring over the climate downturn. Similar statistics have been reported in relation to modern rainfall extremes and related long-term climate modes in the region (e.g., Aryal et al., 2009; Grimm & Tedeschi, 2009; Willems, 2013).

4.2. Climate Downturn Conditions in New Zealand

The simultaneous downturn (KD) in multiple tree-ring proxies (tree-ring width, $\delta^{18}O_{sw,}$ $\delta^{18}O_{cel}$, and $\delta^{13}C_{cel}$) from our kauri chronology suggests that they are all sensitive to the variability of a single (or set of interacting) climate parameters. Based on modern intraannual calibrations of the kauri trees from NZ (Brookman, 2014), we suspect a decline in growing season temperature, concurrent with an increase in relative

humidity and change in precipitation source are responsible for this downturn within the tree-ring and stable isotope signals.

Inter-tree correlations for $\delta^{18}O_{cel}$ are highest during KD (Figure S2) compared to drier and warmer pre-KD and post-KD periods. Previous studies of Late Glacial subfossil trees (Pauly et al., 2018, 2020) have demonstrated stronger inter-tree $\delta^{18}O_{cel}$ correlations during phases of anomalously low $\delta^{18}O_{cel}$ (assumed to be higher precipitation and/or precipitation from a depleted source), likely due to the reduced influence of stomata-driven fractionation on $\delta^{18}O_{cel}$ (Pauly et al., 2020). Indeed, the $\delta^{13}C_{cel}$ demonstrates the lowest inter-tree correlation during the humid KD, suggesting the trees are less sensitive to stomata dynamics controlling $\delta^{13}C_{cel}$ over this interval. While we assume atmospheric conditions are the main driver in kauri stable isotope variability, we cannot rule out groundwater as being another factor modulating sourcewater uptake.

At annual resolution, during the deepest depression in the tree-ring data, $\delta^{18}O_{cel}$ shows low interannual variability (12,520–12,450 cal BP, Figure 2d) and low tree-ring growth. Trees then show an abrupt increase in growth and the interannual variability of $\delta^{18}O_{cel}$ increases considerably (12,450–12,400 cal BP), with instances of interannual $\delta^{18}O$ changes >1‰ increasing by more than threefold. Modern NZ precipitation exhibits extremes every ~2.9 years (Ummenhofer & England, 2007), whereas data in this study show KD extremes at a rate 1 every 12 years and recovery extremes of 1 in every 3–4 years (Figure 2d). Within the Late Glacial context, dendroisotope records from southern France have revealed similar increases in interannual tree-ring $\delta^{18}O$ (+0.2‰ absolute) as a result of the oscillating movement of the polar front at the onset of the Younger Dryas (Pauly et al., 2018).

The similar variability exhibited in modern and ancient kauri tree $\delta^{18}O_{cel}$ and lack of annual or decadal $\delta^{18}O_{cel}$ extremes during the downturn argue against intermittent, flooding as a driver of the depressed tree growth in the region. Furthermore, the tree proxy records do not contain any evidence of flood conditions, which would result in a cessation of growth (rather than a growth depression) as trees would be unable to take up water in anoxic, flooded conditions (Schöngart et al., 2002). Such circumstances have resulted in the destruction of other kauri forests and shortened tree lifespans, leading to swamp preservation of kauri stumps throughout Northland and the Waikato lowlands following extreme storm events (e.g., Boswijk et al., 2005; Green et al., 1985; Ogden et al., 1992). In the case of the kauri in this study, they continued to grow following the depression.

4.3. Combining Climate Model Outputs with Dual-Isotope Theory

Kauri trees thrive in cool and dry summer conditions; yet the trees in this study reveal a prolonged period of unfavorable conditions (moist, cool summers) for kauri growth. Such basic hydroclimate conditions from a modern perspective would be equivalent to a phase of increased La Niña frequency (cold phase of ENSO). However, the climate model (TrACE21ka, Figure 3) output during the downturn offers additional climate variables, providing strong evidence against a prolonged phase of La Niña activity (Table S3).

Kauri tree rings show reduced growth (low tree-ring width) with high humidity (depleted $\delta^{18}O_{cel}$ and $\delta^{13}C_{cel}$) and increased precipitation (depleted $\delta^{18}O_{cel}$ and $\delta^{13}C_{cel}$) during the downturn based on dual-isotope theory (Scheidegger et al., 2000). The TRaCE21ka model provides additional evidence of low temperatures and low sea level pressure conditions being prevalent during the downturn. Together, the model outputs and KAU-ISO reconstructions support the theory of a regional-scale climate deterioration (Palmer et al., 2016).

The model-predicted low sea level pressure, increased southerly airflow (via incoming air masses) and cooler temperatures spanning the downturn are uncharacteristic of La Niña, leaving the period without a clear modern analogue. Rather, it is more likely that sustained low-pressure conditions (Figure 3k) occurred in New Zealand over the downturn. Areas of low pressure (depressions) in the region would lead to high precipitation, low temperatures, and high relative humidity compared to predownturn and postdownturn periods, as evidenced in Figure 3. In particular, weather fronts from the South Ocean (Antarctica) would bring about isotopically depleted rain, creating the continuous depletion in $\delta^{18}O_{cel}$, reflecting sourcewater.

Mean $\delta^{18}O_{cel}$ and $\delta^{13}C_{cel}$ show higher correlations (Figure S2) during and after the downturn compared to before, signifying that the interacting climate variables (temperature, relative humidity, and precipitation) are picked up more strongly in the kauri trees during the extreme climate interval compared to the

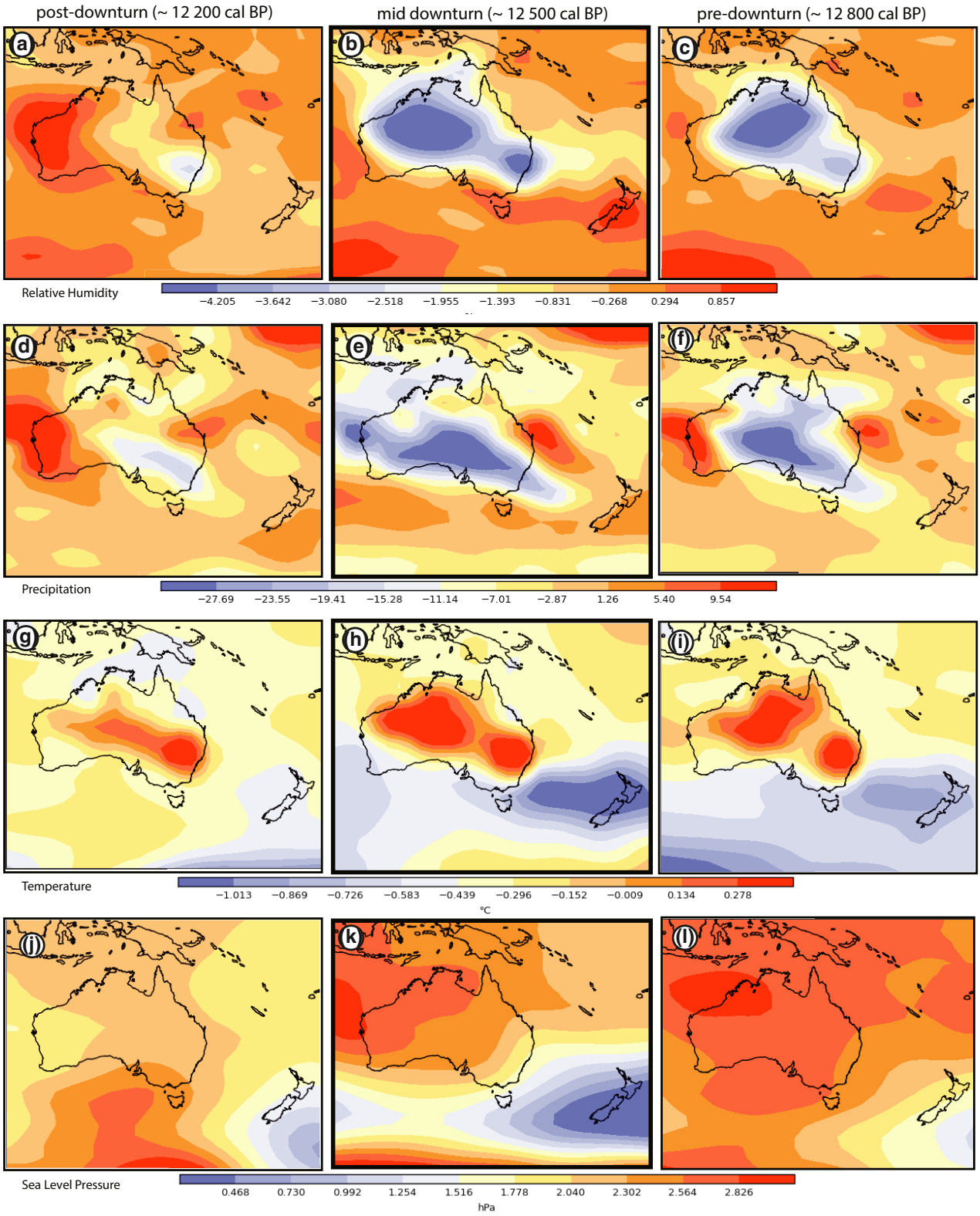

Figure 3. The Late Glacial in the South Pacific demonstrated by coupled atmosphere-ocean general circulation TraCE-21ka. (a–c) Relative humidity, (d–f) precipitation, (g–i) temperature, and (j–l) sea level pressure in three periods: predownturn (12,800 cal BP), middownturn (12,500 cal BP), and postdownturn (12,200 cal BP).

preceding average conditions. Pauly et al. (2020) showed stronger dual isotope correlations in subfossil trees during wetter conditions (higher precipitation, higher humidity) in the NH due to reduced leaf level fractionation (^{18}O enrichment) resulting from partial stomata closure. We expect similar results here as the predownturn period represents average dry conditions in NZ compared to cooler, wetter conditions during and following KD (as recorded in KAU-ISO and TRaCE21ka).

Modern hydroclimate models suggest that anomalous wet years across New Zealand correspond to below average sea surface temperatures and low-sea level pressure across and south of New Zealand (latitude 30–60º band; Ummenhofer & England, 2007), similar to the downturn model output. These conditions have been shown to occur as a result of an alteration in atmospheric circulation, with equatorial shifts in and weakening of the westerlies as well an increase in incoming (south eastern) polar winds (Ummenhofer & England, 2007). Given the similarity between these modern model results and those from this study (in terms of temperature, sea level pressure, and precipitation), we hypothesize the downturn was a result of a similar change in atmospheric circulation. As downturn subsided, westerlies would have theoretically strengthened and moved poleward, warming the 30º–60º latitude band region.

4.4. Proxy Landscape During the Late Glacial

4.4.1. Proxy Records in New Zealand

During KD, coral records in the South Pacific reveal a period of relatively low SST (Corrège et al., 2004), concurrent with a flickering of the Leeuwin Current (De Deckker et al., 2008) impacting flow of westerlies across NZ. Furthermore, a sediment record Lake Hayes in South Island NZ (Hinojosa et al., 2019) recorded a short-term drop in Ca/Ti around 12,500 cal BP (Figure 1e), representing an increase in detrital input and relatively humid/wet conditions (decreased evaporation); compared to the generally dry conditions during the post-ACR interval locally (12,900–11,600 cal BP).

This period of cool, wet conditions occurs at the transition between the local "Late-Glacial cool episode" (NZce-3; 13,740–12,550 cal BP) and the "pre-Holocene amelioration" (NZce-2; 12,550–11,880 cal BP), according to NZ INTIMATE climate event stratigraphy (Barrell et al., 2013; Figure 1i), as described across North Island (Lowe et al., 2008, 2013). Synchronous downward trends in pollen and SST at the onset of NZce-2—reconstructed from an east Tasmanian Sea core (MD06-2991) and Okarito Bog, respectively—suggest an ocean-atmosphere coupling of conditions occurred in the region (Ryan, 2017).

A short-lived, mild depletion in Antarctic ice core $\delta^{18}O$ (Figure 1g) is evident at the time of the KD—particularly in east Antarctic (e.g., Law and Talos; Pedro et al., 2011)—but is difficult to tie to NZ proxy records due to potential dating uncertainties, coarse (multidecadal) temporal resolution as well as the fact that the proxies record different seasons. Given the more complex climate parameters influencing NZ (e.g., polar and subtropical air masses, zonal westerlies) compared to Antarctica, one would expect a higher quantity of climate oscillations occurring in this region compared to those recorded in Antarctic ice cores (Barrell et al., 2013). While a general climate transition between the cool Late Glacial and warm Holocene is clear from the available NZ records, the KAU-ISO record suggests this climate conversion involved a significant and prolonged (multicentennial) hydroclimate shift in NZ. However, the climate drivers and high-resolution dynamics of this interval are difficult to interpret.

4.4.2. Ocean-Atmosphere Teleconnections

An atmospheric $\Delta^{14}C$ rise in the SH has been associated with the onset of the Younger Dryas (increased ^{14}C at ~12,740 cal BP; Hua et al., 2009). This is followed by a few centuries of high variability, including a short-lived peak at ~12,600, concurrent with the onset of KD. Hua et al. (2009) hypothesized that the lack of uniformity between SH terrestrial (Hua et al., 2009), Pacific (Bard et al., 1998, 2004; Burr et al., 1998, 2004; Edwards et al., 1993) and Atlantic (Fairbanks et al., 2005; Hughen et al., 2004) $\Delta^{14}C$ data sets during the early YD peak imply this period initiated as a result of ocean circulation changes rather than ^{14}C (solar) production rate. This delayed peak in tree-ring $\Delta^{14}C$ (compared to marine $\Delta^{14}C$; Hua et al., 2009) is concurrent with the KD onset (this study and Palmer et al., 2016), suggesting the ocean circulation changes may have

driven this climate deterioration recorded in kauri trees on land. This theory is corroborated by the modeled incoming polar winds and related drops sea surface temperature (Figure 3).

While ^{10}Be-modeled Δ^{14}C (representing atmospheric Δ^{14}C unaltered by ocean reservoirs; Hua et al., 2009) underestimates tree-ring Δ^{14}C at the onset of the YD, it closely follows tree-ring Δ^{14}C along the KD timeline a couple centuries later (~12,600–12,400 cal BP). This hints that either (1) solar variability and/or (2) the release of ^{14}C-depleted oceanic CO_2 from the Southern Ocean (Marchitto et al., 2007), likely acted to sustain the climate downturn in New Zealand after the initial (global) ocean circulation trigger, similar to solar variability modulated climate during the Little Ice Age (Gray et al., 2010, and references therein). While the available SH atmospheric CO_2 records from ice cores (e.g., Marcott et al., 2014) are of low temporal resolution (multidecadal) during this interval, they do indicate an increase following the Antarctic Cold Reversal plateau, substantiating the CO_2 release theory. Furthermore, other studies have suggested that climate deteriorations may be amplified through anomalous sea surface temperatures, thereby driving persistent atmospheric circulation states lasting for decades to centuries (van Geel et al., 2003).

5. Conclusions

The subfossil kauri tree-ring width and stable isotopes, in addition to climate model outputs from this study provide further evidence of spring/summer hydroclimate conditions during the YD/GS-1 in the SH, complementing the previously constructed kauri tree-ring width record (Palmer et al., 2016). While the millennial-length Younger Dryas cold reversal is not strongly demonstrated in SH paleoclimate records, variability in tree-ring ^{14}C (Hua et al., 2009) and the Kauri Downturn (this study and Palmer et al., 2016) imply that ocean circulation changes triggered a shorter climate deterioration lasting for at least two and a half centuries (~12,625–12,375 cal BP) over this time interval. Such conditions are generally reflected in regional lake and ocean sediment records, albeit at lower temporal resolution. Despite these promising results, questions remain about what factors drove and modulated the Kauri Downturn and how the NZ hydroclimate regime progressed into the early Holocene climate amelioration.

Data Availability Statement

Decadal stable isotope data are archived on the NOAA ITRDB/WDS Paleo database (https://www.ncdc.noaa.gov/paleo/study/31999).

Acknowledgments
This study was funded by the joint German Research Foundation (DFG, HE3089/9-1 and KR726/10-1). It is a contribution to the climate initiative REKLIM Topic 8 "Abrupt climate change derived from proxy data" of the Helmholtz Association. U. Büntgen received additional funding from the Czech Republic Grant Agency project 17-22102 S.

References

Aryal, S. K., Bates, B. C., Campbell, E. P., Li, Y., Palmer, M. J., & Viney, N. R. (2009). Characterizing and modeling temporal and spatial trends in rainfall extremes. *Journal of Hydrometeorology*, *10*(1), 241–253.

Bard, E., Arnold, M., Hamelin, B., Tisnerat-Laborde, N., & Cabioch, G. (1998). Radiocarbon calibration by means of mass spectrometric 230Th/234U and 14C ages of corals: An updated database including samples from Barbados, Mururoa and Tahiti. *Radiocarbon*, *40*(3), 1085–1092.

Bard, E., Rostek, F., & Ménot-Combes, G. (2004). Radiocarbon calibration beyond 20,000 14C yr BP by means of planktonic foraminifera of the Iberian Margin. *Quaternary Research*, *61*(2), 204–214.

Barrell, D. J., Almond, P. C., Vandergoes, M. J., Lowe, D. J., Newnham, R. M., & INTIMATE members. (2013). A composite pollen-based stratotype for inter-regional evaluation of climatic events in New Zealand over the past 30,000 years (NZ-INTIMATE project). *Quaternary Science Reviews*, *74*, 4–20.

Björck, S., Walker, M. J., Cwynar, L. C., Johnsen, S., Knudsen, K. L., Lowe, J. J., & Wohlfarth, B. (1998). An event stratigraphy for the Last Termination in the North Atlantic region based on the Greenland ice-core record: A proposal by the INTIMATE group. *Journal of Quaternary Science: Published for the Quaternary Research Association*, *13*(4), 283–292.

Blunier, T., Schwander, J., Stauffer, B., Stocker, T., Dällenbach, A., Indermühle, A., et al. (1997). Timing of the Antarctic Cold Reversal and the atmospheric CO_2 increase with respect to the Younger Dryas event. *Geophysical Research Letters*, *24*(21), 2683–2686.

Boswijk, G. (2005). *A history of kauri. Australia and New Zealand Forest Histories* (pp. 19–26). Kingston, Australia: Araucarian Forests, Australian Forest History Society.

Boswijk, G., Fowler, A., Lorrey, A., Palmer, J., & Ogden, J. (2006). Extension of the New Zealand kauri (*Agathis australis*) chronology to 1724 BC. *The Holocene*, *16*(2), 188–199.

Brauer, A., Günter, C., Johnsen, S. J., & Negendank, J. F. (2000). Land-ice teleconnections of cold climatic periods during the last Glacial/Interglacial transition. *Climate Dynamics*, *16*, 229–239.

Brookman, T. H. (2014). *Stable isotope dendroclimatology of New Zealand kauri (Agathis australis* (D. don) lindl.) and cedar (*Libocedrus bidwillii* hook. F.) (PhD thesis). New Zealand: University of Canterbury.

Burr, G. S., Beck, J. W., Taylor, F. W., Récy, J., Edwards, R. L., Cabioch, G., et al. (1998). A high-resolution radiocarbon calibration between 11,700 and 12,400 calendar years BP derived from 230 Th ages of corals from Espiritu Santo Island, Vanuatu. *Radiocarbon*, *40*(3), 1093–1105.

Burr, G. S., Galang, C., Taylor, F. W., Gallup, C., Edwards, R. L., Cutler, K., & Quirk, B. (2004). Radiocarbon results from a 13-kyr BP coral from the Huon Peninsula, Papua New Guinea. *Radiocarbon*, *46*(3), 1211–1224.

Carlson, A. E., & Clark, P. U. (2012). Ice sheet sources of sea level rise and freshwater discharge during the last deglaciation. *Reviews of Geophysics*, *50*, RG4007. https://doi.org/10.1029/2011RG000371

Correge, T., Gagan, M. K., Beck, J. W., Burr, G. S., Cabioch, G., & Le Cornec, F. (2004). Interdecadal variation in the extent of South Pacific tropical waters during the Younger Dryas event. *Nature*, *428*(6986), 927–929.

Crowley, T. J. (1992). North Atlantic deep water cools the Southern Hemisphere. *Paleoceanography*, *7*(4), 489–497.

De Deckker, P., Abed, R. M., De Beer, D., Hinrichs, K. U., O'Loingsigh, T., Schefuß, E., et al. (2008). Geochemical and microbiological fingerprinting of airborne dust that fell in Canberra, Australia, in October 2002. *Geochemistry, Geophysics, Geosystems*, *9*,Q12Q10. https://doi.org/10.1029/2008GC002091

De Deckker, P., Moros, M., Perner, K., & Jansen, E. (2012). Influence of the tropics and southern westerlies on glacial interhemispheric asymmetry. *Nature Geoscience*, *5*(4), 266–269.

Denton, G. H., Anderson, R. F., Toggweiler, J. R., Edwards, R. L., Schaefer, J. M., & Putnam, A. E. (2010). The last glacial termination. *Science*, *328*(5986), 1652–1656.

Ecroyd, C. E. (1982). Biological flora of New Zealand 8. *Agathis australis* (D. Don) Lindl. (Araucariaceae) Kauri. *New Zealand Journal of Botany*, *20*(1), 17–36.

Edwards, T. W. (1993). Interpreting past climate from stable isotopes in continental organic matter. *Geophysical Monograph-American Geophysical Union*, *78*, 333.

Fairbanks, R. G., Mortlock, R. A., Chiu, T. C., Cao, L., Kaplan, A., Guilderson, T. P., et al. (2005). Radiocarbon calibration curve spanning 0 to 50,000 years BP based on paired 230Th/234U/238U and 14C dates on pristine corals. *Quaternary Science Reviews*, *24*(16–17), 1781–1796.

Fowler, A., & Boswijk, G. (2007). Five centuries of ENSO history recorded in *Agathis australis* (kauri) tree rings. *PAGES News*, *15*, 20–21.

Fowler, A., Boswijk, G., & Ogden, J. (2004). Tree-ring studies on *Agathis australis* (kauri): A synthesis of development work on Late Holocene chronologies. *Tree-Ring Research*, *60*(1), 15–29.

Fowler, A., Palmer, J., Salinger, J., & Ogden, J. (2000). Dendroclimatic interpretation of tree-rings in *Agathis australis* (kauri): 2. Evidence of a significant relationship with ENSO. *Journal of the Royal Society of New Zealand*, *30*(3), 277–292.

Fowler, A. M., Boswijk, G., Lorrey, A. M., Gergis, J., Pirie, M., McCloskey, S. P., et al. (2012). Multi-centennial tree-ring record of ENSO-related activity in New Zealand. *Nature Climate Change*, *2*(3), 172–176.

Gray, L. J., Beer, J., Geller, M., Haigh, J. D., Lockwood, M., Matthes, K., et al. (2010). Solar influences on climate. *Reviews of Geophysics*, *48*, RG4001. https://doi.org/10.1029/2009RG000282

Green, J. D., & Lowe, D. J. (1985). Stratigraphy and development of c. 17 000 year old Lake Maratoto, North Island, New Zealand, with some inferences about postglacial climatic change. *New Zealand Journal of Geology and Geophysics*, *28*(4), 675–699.

Grimm, A. M., & Tedeschi, R. G. (2009). ENSO and extreme rainfall events in South America. *Journal of Climate*, *22*(7), 1589–1609.

Hajdas, I., Lowe, D. J., Newnham, R. M., & Bonani, G. (2006). Timing of the late-glacial climate reversal in the Southern Hemisphere using high-resolution radiocarbon chronology for Kaipo bog, New Zealand. *Quaternary Research*, *65*(2), 340–345.

Hinojosa, J. L., Moy, C. M., Vandergoes, M., Feakins, S. J., & Sessions, A. L. (2019). Hydrologic change in New Zealand during the last deglaciation linked to reorganization of the Southern Hemisphere westerly winds. *Paleoceanography and Paleoclimatology*, *34*, 2158–2170. https://doi.org/10.1029/2019PA003656

Hogg, A., Southon, J., Turney, C., Palmer, J., Ramsey, C. B., Fenwick, P., et al. (2016). Decadally resolved lateglacial radiocarbon evidence from New Zealand kauri. *Radiocarbon*, *58*(4), 709–733. https://doi.org/10.1017/RDC.2016.86

Hua, Q., Barbetti, M., Fink, D., Kaiser, K. F., Friedrich, M., Kromer, B., et al. (2009). Atmospheric 14C variations derived from tree rings during the early Younger Dryas. *Quaternary Science Reviews*, *28*(25–26), 2982–2990.

Hughen, K. A., Baillie, M. G., Bard, E., Beck, J. W., Bertrand, C. J., Blackwell, P. G., et al. (2004). Marine04 marine radiocarbon age calibration, 0–26 cal kyr BP. *Radiocarbon*, *46*(3), 1059–1086.

Kaplan, M. R., Schaefer, J. M., Denton, G. H., Barrell, D. J., Chinn, T. J., Putnam, A. E., et al. (2010). Glacier retreat in New Zealand during the Younger Dryas stadial. *Nature*, *467*(7312), 194–197.

Kawamura, K., Parrenin, F., Lisiecki, L., Uemura, R., Vimeux, F., Severinghaus, J. P., et al. (2007). Northern Hemisphere forcing of climatic cycles in Antarctica over the past 360,000 years. *Nature*, *448*(7156), 912–916.

Lauterbach, S., Brauer, A., Andersen, N., Danielopol, D. L., Dulski, P., Hüls, M., et al. (2011). Environmental responses to Lateglacial climatic fluctuations recorded in the sediments of pre-Alpine Lake Mondsee (northeastern Alps). *Journal of Quaternary Science*, *26*(3), 253–267.

Liñán, I. D., Gutiérrez, E., Helle, G., Heinrich, I., Andreu-Hayles, L., Planells, O., et al. (2011). Pooled versus separate measurements of tree-ring stable isotopes. *Science of the Total Environment*, *409*(11), 2244–2251.

Lorrey, A. M., Boswijk, G., Hogg, A., Palmer, J. G., Turney, C. S., Fowler, A. M., et al. (2018). The scientific value and potential of New Zealand swamp kauri. *Quaternary Science Reviews*, *183*, 124–139.

Lorrey, A. M., Brookman, T. H., Evans, M. N., Fauchereau, N. C., Macinnis-Ng, C., Barbour, M. M., et al. (2016). Stable oxygen isotope signatures of early season wood in New Zealand kauri (*Agathis australis*) tree rings: Prospects for palaeoclimate reconstruction. *Dendrochronologia*, *40*, 50–63.

Lorrey, A. M., & Ogden, J. (2005). Tree-ring analysis of subfossil kauri (Agathis australis) from Omaha Flats, Tawharunui Peninsula, New Zealand. New Zealand Tree-Ring Site Report, 22, School of Geography and Environmental Science Working Paper 32.

Lowe, D. J., Blaauw, M., Hogg, A. G., & Newnham, R. M. (2013). Ages of 24 widespread tephras erupted since 30,000 years ago in New Zealand, with re-evaluation of the timing and palaeoclimatic implications of the Lateglacial cool episode recorded at Kaipo bog. *Quaternary Science Reviews*, *74*, 170–194.

Lowe, D. J., Shane, P. A., Alloway, B. V., & Newnham, R. M. (2008). Fingerprints and age models for widespread New Zealand tephra marker beds erupted since 30,000 years ago: A framework for NZ-INTIMATE. *Quaternary Science Reviews*, *27*(1–2), 95–126.

Marchitto, T. M., Lehman, S. J., Ortiz, J. D., Flückiger, J., & van Geen, A. (2007). Marine radiocarbon evidence for the mechanism of deglacial atmospheric CO_2 rise. *Science*, *316*(5830), 1456–1459.

Marcott, S. A., Bauska, T. K., Buizert, C., Steig, E. J., Rosen, J. L., Cuffey, K. M., et al. (2014). Centennial-scale changes in the global carbon cycle during the last deglaciation. *Nature*, *514*(7524), 616–619.

Merkt, J., & Müller, H. (1999). Varve chronology and palynology of the Lateglacial in Northwest Germany from lacustrine sediments of Hämelsee in Lower Saxony. *Quaternary International*, *61*(1), 41–59.
Newnham, R. M., & Lowe, D. J. (2000). Fine-resolution pollen record of late-glacial climate reversal from New Zealand. *Geology*, *28*(8), 759–762.
Ogden, J., & Ahmed, M. (1989). Climate response function analyses of kauri (*Agathis australis*) tree-ring chronologies in northern New Zealand. *Journal of the Royal Society of New Zealand*, *19*(2), 205–221.
Ogden, J., Wilson, A., Hendy, C., Newnham, R. M., & Hogg, A. G. (1992). The late Quaternary history of kauri (*Agathis australis*) in New Zealand and its climatic significance. *Journal of Biogeography*, *19*(6), 611–622. https://doi.org/10.2307/2845704
Palmer, J. G., Turney, C. S., Cook, E. R., Fenwick, P., Thomas, Z., Helle, G., et al. (2016). Changes in El Niño–Southern Oscillation (ENSO) conditions during the Greenland Stadial 1 (GS-1) chronozone revealed by New Zealand tree-rings. *Quaternary Science Reviews*, *153*, 139–155.
Palmer, J., Turney, C., Cook, E., Fenwick, P., Thomas, Z., Helle, G. et al. (2017). Changes in El Nino-Southern Oscillation (ENSO) conditions during the Younger Dryas revealed by New Zealand tree-rings. *EGUGA*, 6717.
Paul, D., Skrzypek, G., & Fórizs, I. (2007). Normalization of measured stable isotopic compositions to isotope reference scales—A review. *Rapid Communications in Mass Spectrometry*, *21*(18), 3006–3014.
Pauly, M., Helle, G., Büntgen, U., Wacker, L., Treydte, K., Reinig, F., et al. (2020). Tree-ring stable isotopes from Swiss subfossil pines reveal Late Glacial climate variability over the North Atlantic/European sector. *Quaternary Science Reviews*, *247*, 106550.
Pauly, M., Helle, G., Miramont, C., Büntgen, U., Treydte, K., Reinig, F., et al. (2018). Subfossil trees suggest enhanced Mediterranean hydroclimate variability at the onset of the Younger Dryas. *Scientific Reports*, *8*(1), 13980. https://doi.org/10.1038/s41598-018-32251-2
Pedro, J. B., Van Ommen, T. D., Rasmussen, S. O., Morgan, V. I., Chappellaz, J., Moy, A. D., et al. (2011). The last deglaciation: Timing the bipolar seesaw. *Climate of the Past*, *7*, 671–683.
Rach, O., Brauer, A., Wilkes, H., & Sachse, D. (2014). Delayed hydrological response to Greenland cooling at the onset of the Younger Dryas in western Europe. *Nature Geoscience*, *7*(2), 109–112.
Rasmussen, S. O., Bigler, M., Blockley, S. P., Blunier, T., Buchardt, S. L., Clausen, H. B., et al. (2014). A stratigraphic framework for abrupt climatic changes during the Last Glacial period based on three synchronized Greenland ice-core records: Refining and extending the INTIMATE event stratigraphy. *Quaternary Science Reviews*, *106*, 14–28.
Renssen, H., Mairesse, A., Goosse, H., Mathiot, P., Heiri, O., Roche, D. M., et al. (2015). Multiple causes of the Younger Dryas cold period. *Nature Geoscience*, *8*(12), 946–949.
Ryan, M. T. (2017). *Late Quaternary vegetation and climate history reconstructed from palynology of marine cores off southwestern New Zealand (PhD thesis).*. Wellington, New Zealand: Victoria University of Wellington.
Scheidegger, Y., Saurer, M., Bahn, M., & Siegwolf, R. (2000). Linking stable oxygen and carbon isotopes with stomatal conductance and photosynthetic capacity: a conceptual model. *Oecologia*, *125*(3), 350–357.
Schollaen, K., Baschek, H., Heinrich, I., Slotta, F., Pauly, M., & Helle, G. (2017). A guideline for sample preparation in modern tree-ring stable isotope research. *Dendrochronologia*, *44*, 133–145.
Schöngart, J., Piedade, M. T. F., Ludwigshausen, S., Horna, V., & Worbes, M. (2002). Phenology and stem-growth periodicity of tree species in Amazonian floodplain forests. *Journal of Tropical Ecology*, 18(4), 581–597.
Steffensen, J. P., Andersen, K. K., Bigler, M., Clausen, H. B., Dahl-Jensen, D., Fischer, H., et al. (2008). High-resolution Greenland ice core data show abrupt climate change happens in few years. *Science*, *321*(5889), 680–684.
Stocker, T. F. (1998). The seesaw effect. *Science*, *282*(5386), 61–62.
Turney, C. S., Fifield, L. K., Hogg, A. G., Palmer, J. G., Hughen, K., Baillie, M. G., et al. (2010). The potential of New Zealand kauri (*Agathis australis*) for testing the synchronicity of abrupt climate change during the Last Glacial Interval (60,000–11,700 years ago). *Quaternary Science Reviews*, *29*(27–28), 3677–3682.
Ummenhofer, C. C., & England, M. H. (2007). Interannual extremes in New Zealand precipitation linked to modes of Southern Hemisphere climate variability. *Journal of Climate*, *20*(21), 5418–5440.
van Geel, B., Buurman, J., Brinkkemper, O., Schelvis, J., Aptroot, A., van Reenen, G., & Hakbijl, T. (2003). Environmental reconstruction of a Roman Period settlement site in Uitgeest (The Netherlands), with special reference to coprophilous fungi. *Journal of Archaeological Science*, *30*(7), 873–883.
von Grafenstein, U., Erlenkeuser, H., Brauer, A., Jouzel, J., & Johnsen, S. J. (1999). A mid-European decadal isotope-climate record from 15,500 to 5000 years BP. *Science*, *284*(5420), 1654–1657.
WAIS Divide Project Members. (2015). Precise interpolar phasing of abrupt climate change during the last ice age. *Nature*, *520*(7549), 661.
Wieloch, T., Helle, G., Heinrich, I., Voigt, M., & Schyma, P. (2011). A novel device for batch-wise isolation of α-cellulose from small-amount wholewood samples. *Dendrochronologia*, *29*(2), 115–117.
Willems, P. (2013). Adjustment of extreme rainfall statistics accounting for multidecadal climate oscillations. *Journal of Hydrology*, *490*, 126–133.

References From the Supporting Information

Araguás-Araguás, L., Froehlich, K., & Rozanski, K. (2000). Deuterium and oxygen-18 isotope composition of precipitation and atmospheric moisture. *Hydrological Processes*, *14*(8), 1341–1355.
Dansgaard, W. (1964). Stable isotopes in precipitation. *Tellus*, *16*(4), 436–468.https://doi.org/10.1111/j.2153-3490.1964.tb00181.x
Gat, J. R. (2000). Atmospheric water balance—The isotopic perspective. *Hydrological Processes*, *14*(8), 1357–1369.
Kahmen, A., Sachse, D., Arndt, S. K., Tu, K. P., Farrington, H., Vitousek, P. M., & Dawson, T. E. (2011). Cellulose $\delta^{18}O$ is an index of leaf-to-air vapor pressure difference (VPD) in tropical plants. *Proceedings of the National Academy of Sciences of the United States of America*, *108*(5), 1981–1986.
Lüttge, U., & Kluge, M. (2012). *Botanik: Die einführende Biologie der Pflanzen.*. Hoboken, NJ: John Wiley & Sons.
Palmer, J., & Ogden, J. (1983). A dendrometer band study of the seasonal pattern of radial increment in kauri (*Agathis australis*). *New Zealand Journal of Botany*, *21*(2), 121–125.
Saurer, M., Kress, A., Leuenberger, M., Rinne, K. T., Treydte, K. S., & Siegwolf, R. T. (2012). Influence of atmospheric circulation patterns on the oxygen isotope ratio of tree rings in the Alpine region. *Journal of Geophysical Research*, *117*, D05118. https://doi.org/10.1029/2011JD016861

Schollaen, K., Heinrich, I., Neuwirth, B., Krusic, P. J., D'Arrigo, R. D., Karyanto, O., & Helle, G. (2013). Multiple tree-ring chronologies (ring width, $\delta^{13}C$ and $\delta^{18}O$) reveal dry and rainy season signals of rainfall in Indonesia. *Quaternary Science Reviews*, *73*, 170–181.

Xu, C., Ge, J., Nakatsuka, T., Yi, L., Zheng, H., & Sano, M. (2016). Potential utility of tree ring $\delta^{18}O$ series for reconstructing precipitation records from the lower reaches of the Yangtze River, southeast China. *Journal of Geophysical Research: Atmospheres*, *121*, 3954–3968. https://doi.org/10.1002/2015JD023610